

Hall anomalies in the centrosymmetric triangular-lattice antiferromagnet GdGa2

Sidi Wang(王思迪), Jiyuan Li(李纪源), Yuhao Wang(王宇豪), Keqi Xia(夏克奇), Jing Meng(孟婧), Bocheng Yu(余博丞), Yiqian Hu(胡艺骞), Zheng Li(李峥), Hui Zhang(张慧), Jingzhong Luo(罗晶中), Dongmei Jiang(蒋冬梅), Qingfeng Zhan(詹清峰), Tian Shang(商恬), and Yang Xu(徐杨)

Citation: Chin. Phys. B, 2026, 35 (**2**): 027502. DOI: 10.1088/1674-1056/ae2672
http://cpb.iphy.ac.cn; http://iopscience.iop.org/cpb

What follows is a list of articles you may be interested in

Crystal structure, magnetic properties, and tunable Kondo effect in a new compound Nd5ScSb12

Yi-Ran Li(李祎冉), Na Li(李娜), Ping Su(苏平), Hui Liang(梁慧), Kai-Yuan Hu(胡开源), Ying Zhou(周颖), Dan-Dan Wu(吴丹丹), Yan Sun(孙燕), Qiu-Ju Li(李秋菊), Xia Zhao(赵霞), Xue-Feng Sun(孙学峰), and Yi-Yan Wang(王义炎)
Chin. Phys. B, 2025, 34 (**6**): 067502. DOI: 10.1088/1674-1056/adc2df

Valley modulation and topological phase transition in staggered kagome ferromagnets

Yuheng Xing(邢玉恒), Wenjuan Qiu(邱文娟), Xinxing Wu(吴新星), and Yue Tan(谭悦)
Chin. Phys. B, 2024, 33 (**12**): 127503. DOI: 10.1088/1674-1056/ad7af7

Induced magneto-conductivity in a two-node Weyl semimetal under Gaussian random disorder

Chuanxiong Xu(徐川雄), Haoping Yu(于昊平), Mei Zhou(周梅), and Xuanting Ji(吉轩廷)
Chin. Phys. B, 2024, 33 (**9**): 097502. DOI: 10.1088/1674-1056/ad59fc

Tailoring-compensated ferrimagnetic state and anomalous Hall effect in quaternary Mn-Ru-V-Ga Heusler compounds

Jin-Jing Liang(梁瑾静), Xue-Kui Xi(郗学奎), Wen-Hong Wang(王文洪), and Yong-Chang Lau(刘永昌)
Chin. Phys. B, 2024, 33 (**7**): 077504. DOI: 10.1088/1674-1056/ad34c8

Enhanced anomalous Hall effect in kagome magnet YbMn6Sn6 with intermediate-valence ytterbium

Longfei Li(李龙飞), Shengwei Chi(迟晟玮), Wenlong Ma(马文龙), Kaizhen Guo(郭凯臻), Gang Xu(徐刚), and Shuang Jia(贾爽)
Chin. Phys. B, 2024, 33 (5): 057501. DOI: 10.1088/1674-1056/ad322d

---

RAPID COMMUNICATION

Hall anomalies in the centrosymmetric triangular-lattice antiferromagnet $GdGa_2$

Sidi Wang(王思迪), Jiyuan Li(李纪源), Yuhao Wang(王宇豪), Keqi Xia(夏克奇), Jing Meng(孟婧), Bocheng Yu(余博丞), Yiqian Hu(胡艺骞), Zheng Li(李峥), Hui Zhang(张慧), Jingzhong Luo(罗晶中), Dongmei Jiang(蒋冬梅), Qingfeng Zhan(詹清峰), Tian Shang(商恬)[†], and Yang Xu(徐杨)[‡]

Key Laboratory of Polar Materials and Devices (MOE), School of Physics, East China Normal University, Shanghai 200241, *China*

(Received 14 September 2025; revised manuscript received 22 November 2025; accepted manuscript online 2 December 2025)

Skyrmions emerging in centrosymmetric materials have garnered significant interest. $GdGa_2$, a recently discovered centrosymmetric antiferromagnet with a triangular lattice, has been proposed to host possible Néel-type skyrmions exhibiting an extremely short magnetic periodicity in the so-called A-phases. Here, we report the magnetic and magnetotransport properties of $GdGa_2$ single crystals. Hall anomalies beyond magnetization scaling emerge at intermediate magnetic fields, coinciding with the skyrmion-hosting A-phases. The small amplitude of the Hall anomalies may be attributed to the short period of the spin textures. In contrast, the transport behavior of $TbGa_2$ single crystals is well described by a conventional two-band model. This discrepancy likely arises from distinct Ruderman–Kittel–Kasuya–Yosida interaction strengths and/or magnetic anisotropy between the two crystals. Our results establish $GdGa_2$ as a new material platform for the exploration of skyrmion physics in centrosymmetric systems.

Keywords: skyrmions in centrosymmetric materials, rare-earth antiferromagnets, topological Hall effect

PACS: 75.47.–m, 12.39.Dc, 71.20.Eh

DOI: 10.1088/1674-1056/ae2672 **CSTR:** 32038.14.CPB.ae2672

1. Introduction

Magnetic systems with a triangular lattice offer a fertile playground for the exploration of a host of quantum phenomena, e.g., quantum criticality, quantum spin liquids, and skyrmions.[1–3] Magnetic skyrmions — vortex-like nanoscale spin textures — have attracted significant research interest due to their potential applications in next-generation spintronic devices and information storage technologies.[4–7] Conventionally, skyrmions are stabilized by the Dzyaloshinskii–Moriya interaction in non-centrosymmetric materials,[8–10] but have recently been observed in centrosymmetric systems where competing magnetic interactions enable their formation.[11] Notable examples include tetragonal Eu(Al, Ga)$_4$[12–15], $GdRu_2Si_2$,[16,17] and the breathing-kagome compound $Gd_3Ru_4Al_{12}$.[18,19] Another Gd-based compound, Gd_2PdSi_3 with a triangular lattice, has also been identified as a typical material hosting a skyrmion lattice.[20,21] In these centrosymmetric Eu- or Gd-based materials, skyrmion stabilization mechanisms primarily involve magnetic anisotropy and frustration. Here, exchange frustration may be facilitated by geometric aspects (kagome and tetragonal lattices) and can exhibit either short-range or long-range Ruderman–Kittel–Kasuya–Yosida (RKKY) character.[22,23] Hall resistivity measurements serve as critical probes for detecting such non-trivial spin textures, as skyrmions endow the electron wavefunction with a finite Berry phase that manifests as a topological contribution to the transverse transport.[24]

REGa_2 (*RE* = Gd, Tb) compounds are centrosymmetric frustrated magnets with triangular lattices. Recent resonant elastic x-ray scattering (REXS) measurements on $GdGa_2$ revealed a complex superposition of various cycloidal spin textures, possibly in the form of skyrmion lattices exhibiting an extremely short magnetic periodicity (0.54 nm) within the A-phases ($T_N < 25$ K, 3 T $< \mu_0 H <$ 7 T), suggesting potential for ultrahigh-density storage applications.[25] However, transport evidence of skyrmions in $GdGa_2$ remains lacking. Here, we present systematic magnetization, longitudinal resistivity, and Hall resistivity measurements of *RE*Ga_2 single crystals. Anomalies beyond the ordinary Hall contribution and the conventional anomalous Hall contribution with magnetization scaling are identified in the Hall resistivity of $GdGa_2$, with a typical amplitude of ~ 0.07 μΩ·cm. The phase region exhibiting such a finite topological Hall contribution corresponds to part of the A-phases determined by REXS experiments. In contrast, no comparable anomalies are detected in the Hall resistivity of $TbGa_2$, which is well described by a two-band model of the ordinary Hall effect. We discuss the implications of our results for the study of skyrmions in centrosymmetric rare-earth magnets.

[†]Corresponding author. E-mail: tshang@phy.ecnu.edu.cn

[‡]Corresponding author. E-mail: yxu@phy.ecnu.edu.cn

© 2026 Chinese Physical Society and IOP Publishing Ltd. All rights, including for text and data mining, AI training, and similar technologies, are reserved.

2. Experimental details

Single crystals of $GdGa_2$ and $TbGa_2$ were grown via the Pb-flux method.[26] High-purity Gd/Tb, Ga, and Pb were combined in a 1 : 2 : 10 molar ratio in an alumina crucible, sealed in an Ar-filled quartz tube. The mixture was heated to 1000 °C for 10 h and then cooled to 400 °C at 1 °C·min^{-1}. To obtain sizable crystals, thermal cycling was implemented: heating to 850 °C (120 min), cooling to 400 °C (1 °C·min^{-1}), reheating to 700 °C (1 °C·min^{-1}), and final cooling to 400 °C (1 °C·min^{-1}). Centrifugation at 400 °C removed the Pb flux, yielding high-quality plate-like single crystals (typical dimensions: $\sim 1 \times 1 \times 0.1$ mm^3) as shown in Fig. 1(b) inset.

Crystal orientation and phase purity were characterized by x-ray diffraction (XRD) using a PANalytical X'Pert Pro x-ray diffractometer with Cu $K\alpha$ radiation. Rietveld refinement of powder XRD patterns was performed using the FullProf suite. Electrical transport properties were measured using a cryogen-free magnets property measurement system. Magnetic properties were characterized with a Quantum Design magnetic property measurement system. For all measurements, the magnetic field was applied parallel to the c-axis ($H \parallel c$), while electrical transport measurements employed current within the ab-plane ($I \parallel ab$) using a four-probe direct current (DC) configuration with 10 mA current.

To eliminate spurious contributions to transport measurements arising from non-ideal Hall contact alignment, the longitudinal component of the Hall resistivity ρ_{xy} was removed via antisymmetrization: $\rho_{xy}(H) = (\rho_{xy}(H) - \rho_{xy}(-H))/2$. Conversely, for the longitudinal resistivity ρ_{xx}, the extraneous transverse contribution was eliminated through symmetrization: $\rho_{xx}(H) = (\rho_{xx}(H) + \rho_{xx}(-H))/2$.

3. Results and discussion

3.1. Crystal structure

REGa_2 compounds crystallize in a centrosymmetric hexagonal AlB_2-type structure, featuring alternating triangular lattice rare-earth and honeycomb Ga atomic layers along the c-axis (Fig. 1(a)). This geometrically frustrated configuration promotes competing magnetic interactions that may stabilize unconventional magnetic ground states.[27]

The phase purity and crystal structure of the synthesized *RE*Ga_2 single crystals were verified by room-temperature powder XRD. Samples prepared under identical conditions exhibit consistent structural characteristics, with $GdGa_2$ selected as the representative system for detailed analysis. Powder XRD with Rietveld refinement confirmed the phase purity of $GdGa_2$ and quantified the phase composition, revealing a dominant $GdGa_2$ mass fraction of 97.16% with trace surface Pb residues (2.84%) from the flux (Fig. 1(b), top). Refinement identified these Pb impurities, with characteristic peaks clearly labeled in XRD data collected on both the powder (top) and single crystal (bottom) of Fig. 1(b). XRD data collected on the single crystal revealed prominent (00l) reflections, indicating that the sample surface normal is aligned with the c-axis. These minor Pb impurities have a negligible impact due to their low superconducting critical fields (< 0.1 T) and their removal via surface polishing prior to transport and magnetic measurements.

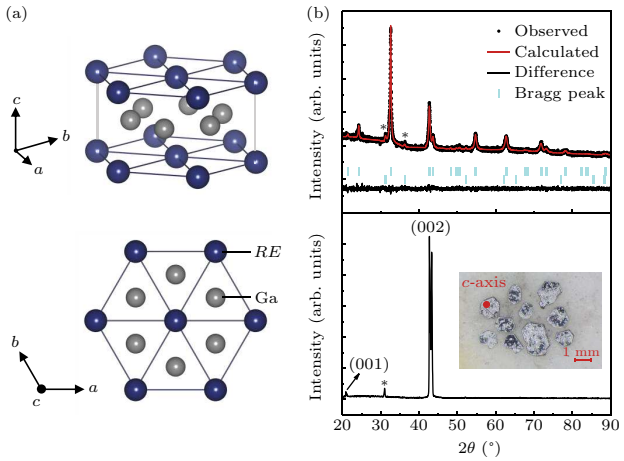


Fig. 1. (a) Crystal structure of *RE*Ga_2 viewed perpendicular to (top) and along (bottom) the c-axis. *RE* and Ga atoms are denoted by blue and grey spheres, respectively. (b) Top: Room-temperature powder XRD pattern and Rietveld refinement of $GdGa_2$. The black circles represent the observed data, the red line represents the fitted pattern, the black line represents the difference between the observed and calculated intensities, and the blue bars indicate the Bragg peak positions. Bottom: Single-crystal XRD pattern confirming the (00l) orientation of the largest natural surface. Asterisks mark Pb-derived impurity peaks. Inset: Optical image of hexagonal crystals, showing the ab-plane.

3.2. Transport and magnetic properties of *RE*Ga_2 (*RE* = Gd, Tb)

The temperature-dependent electrical resistivity ρ and magnetic susceptibility χ were characterized for $GdGa_2$ and $TbGa_2$. Both compounds exhibit metallic behavior and undergo a paramagnetic-to-antiferromagnetic transition upon cooling, as evidenced in Fig. 2.

For $GdGa_2$, the resistivity ρ decreases gradually between 2–50 K due to diminishing magnetic scattering as magnetic moments progressively order. At $T_N = 15$ K, ρ exhibits an anomaly (indicated by arrows in Fig. 2(a)). This transition temperature coincides with a sharp anomaly in the magnetic susceptibility $\chi(T)$ (Fig. 2(b)), suggesting the onset of a magnetic phase transition, which is subsequently identified as antiferromagnetic ordering based on the negative Curie–Weiss temperature (discussed below). The lower T_N compared to $T_N = 25$ K reported in the literature is attributed to different growth conditions.[25] A second resistivity anomaly emerges at $T_t = 6$ K, consistent with prior reports,[28] signifying a spin reorientation within the antiferromagnetic phase as confirmed by neutron diffraction.[29] No corresponding anomaly in $\chi(T)$ is observed at T_t. The inset of Fig. 2(b) displays the inverse

susceptibility $\chi(T)^{-1}$. Linear fitting was performed according to the Curie–Weiss law

$$\chi = \frac{C}{T-\theta_{\rm p}}, \tag{1}$$

where C is the Curie constant and $\theta_{\rm p}$ is the paramagnetic Curie temperature. The fitted $\theta_{\rm p} = -105.9$ K confirms dominant antiferromagnetic interactions.

$TbGa_2$ exhibits no discernible resistivity anomaly. However, magnetic susceptibility $\chi(T)$ measurements reveal an antiferromagnetic transition at $T_{\rm N} = 15$ K (Figs. 2(c) and 2(d)). The Curie–Weiss fit to $\chi(T)^{-1}$ in the inset of Fig. 2(d) yields $\theta_{\rm p} = -149.1$ K, further confirming dominant antiferromagnetic interactions.

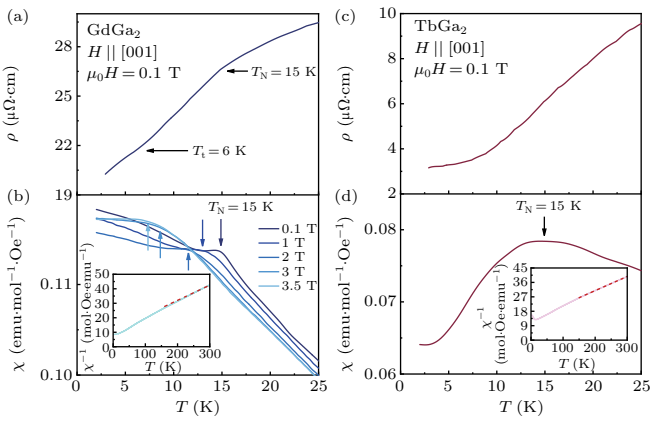


Fig. 2. Electrical and magnetic properties of $GdGa_2$ and $TbGa_2$ under an applied magnetic field. (a) Electrical resistivity $\rho(T)$ of $GdGa_2$. (b) Magnetic susceptibility $\chi(T)$ of $GdGa_2$ measured under zero-field cooling. Inset: Curie–Weiss fit (dashed line). (c) Electrical resistivity $\rho(T)$ of $TbGa_2$. (d) Magnetic susceptibility $\chi(T)$ of $TbGa_2$ measured under zero-field cooling. Inset: Curie–Weiss fit (dashed line).

Comprehensive field-dependent magnetization $M(H)$, longitudinal resistivity $\rho_{xx}(H)$, and Hall resistivity $\rho_{xy}(H)$ measurements were performed on $GdGa_2$ and $TbGa_2$ single crystals. Data were acquired with the magnetic field applied parallel to the crystallographic c-axis ($H \parallel c$), as presented in Fig. 3.

$GdGa_2$ exhibits unsaturated magnetization $M(H)$ in both the paramagnetic and antiferromagnetic states (Fig. 3(a)). The nonlinear Hall resistivity ρ_{xy} in the paramagnetic phase (e.g. $T = 18$ K $> T_{\rm N}$) suggests multicarrier transport (Fig. 3(b)), consistent with the de Haas–van Alphen effect.[28] To verify this interpretation, $\rho_{xx}(H)$ and $\rho_{xy}(H)$ were simultaneously fitted using a two-band model

$$\rho_{xx}(H) = \frac{1}{e}\frac{(n_{\rm h}\mu_{\rm h}+n_{\rm e}\mu_{\rm e})+(n_{\rm h}\mu_{\rm e}+n_{\rm e}\mu_{\rm h})\mu_{\rm h}\mu_{\rm e}H^2}{(n_{\rm h}\mu_{\rm h}+n_{\rm e}\mu_{\rm e})^2+(n_{\rm h}-n_{\rm e})^2\mu_{\rm h}^2\mu_{\rm e}^2H^2}, \tag{2}$$

$$\rho_{xy}(H) = \frac{H}{e}\frac{(n_{\rm h}\mu_{\rm h}^2-n_{\rm e}\mu_{\rm e}^2)+(n_{\rm h}-n_{\rm e})\mu_{\rm h}^2\mu_{\rm e}^2H^2}{(n_{\rm h}\mu_{\rm h}+n_{\rm e}\mu_{\rm e})^2+(n_{\rm h}-n_{\rm e})^2\mu_{\rm h}^2\mu_{\rm e}^2H^2}, \tag{3}$$

where $n_{\rm h}$ ($n_{\rm e}$) and $\mu_{\rm h}$ ($\mu_{\rm e}$) denote the hole (electron) density and mobility. At $T = 18$ K ($T > T_{\rm N}$), the model describes the data well (red dashed curves, Figs. 3(b) and 3(d)). In contrast, at $T = 2$ K (the antiferromagnetically ordered state), $M(H)$, $\rho_{xy}(H)$, and $\rho_{xx}(H)$ display kinks around $\mu_0 H \sim 4$ T (Figs. 3(a), 3(c), and 3(d)), preventing a global two-band fitting over the entire 0–7 T field range. This behavior likely originates from spin textures that modify electron dynamics. Consequently, the anomalous 2.5–5.5 T region was excluded, and segmented two-band fits were performed (see Fig. 3),[26] allowing reliable extraction of the transport parameters ($n_{\rm h}$, $n_{\rm e}$, $\mu_{\rm h}$, and $\mu_{\rm e}$) from the unaffected field ranges. The low-temperature anomalies will be analyzed in detail in the next section.

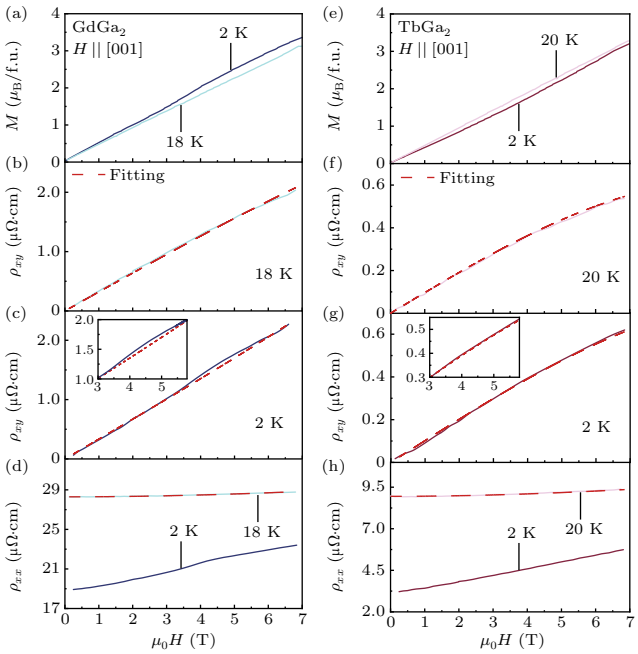


Fig. 3. (a)–(d) Field-dependent (a) magnetization $M(H)$, (b) Hall resistivity $\rho_{xy}(H)$ at $T = 18$ K, (c) Hall resistivity $\rho_{xy}(H)$ at $T = 2$ K, with the inset showing a zoomed-in view of the intermediate-field data, and (d) longitudinal resistivity $\rho_{xx}(H)$ of $GdGa_2$ at selected temperatures ($H \parallel c$). Dashed curves: two-band fits at selected temperatures using Eqs. (2) and (3). (e)–(h) Corresponding (e) $M(H)$, (f) $\rho_{xy}(H)$ at $T = 20$ K, (g) $\rho_{xy}(H)$ at $T = 2$ K, with the inset showing a zoomed-in view of the intermediate-field data, and (h) $\rho_{xx}(H)$ of $TbGa_2$. Dashed curves: two-band fits at selected temperatures.

Similar to $GdGa_2$, $TbGa_2$ exhibits unsaturated magnetization $M(H)$ in both the paramagnetic and antiferromagnetic states (Fig. 3(e)). At $T = 20$ K ($T > T_{\rm N}$), both the Hall resistivity $\rho_{xy}(H)$ and the longitudinal resistivity $\rho_{xx}(H)$ display nonlinear field dependence over the range 0–7 T, which is well described by the two-band model (red dashed curves in Figs. 3(f) and 3(h)). In the magnetically ordered state at $T = 2$ K, no kinks are observed in $M(H)$, $\rho_{xy}(H)$, or $\rho_{xx}(H)$ over the full field range, and the data remain equally well described by the two-band model (red dashed curves in Fig. 3(g)). Consequently, global two-band fitting yields the parameters ($n_{\rm h}$, $n_{\rm e}$, $\mu_{\rm h}$, and $\mu_{\rm e}$) throughout the investigated temperature and field regimes.

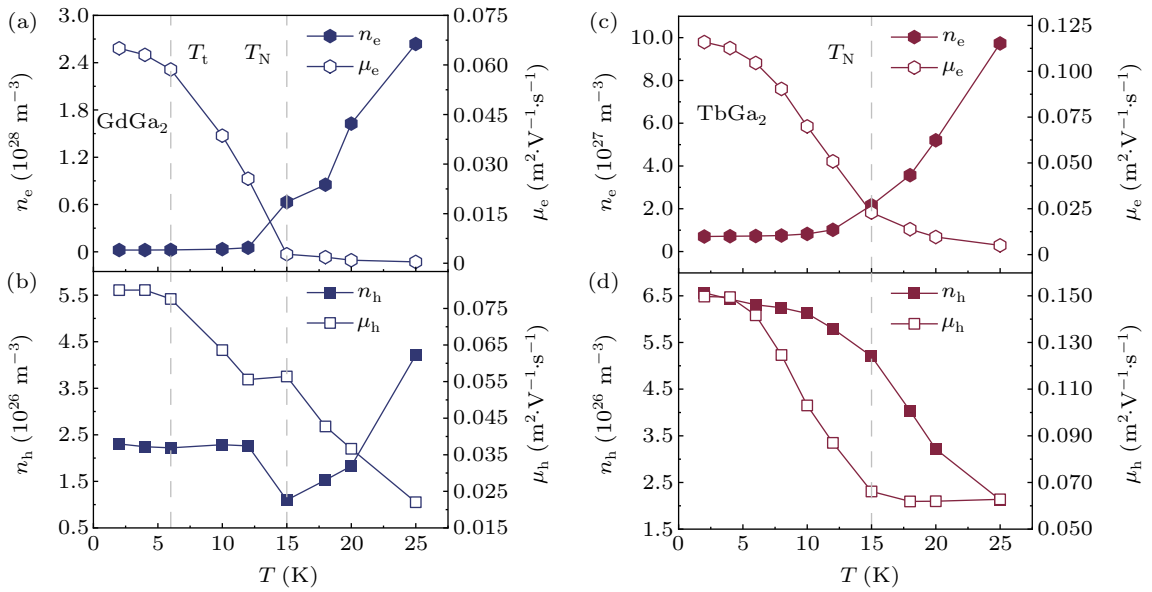


Fig. 4. Temperature-dependent parameters obtained from two-band fitting. Dashed vertical lines denote the magnetic transition temperatures T_N or T_t. (a) Electron density n_e and mobility μ_e for $GdGa_2$. (b) Hole density n_h and mobility μ_h for $GdGa_2$. (c) Electron density n_e and mobility μ_e for $TbGa_2$. (d) Hole density n_h and mobility μ_h for $TbGa_2$.

The fitted parameters (n_h, n_e, μ_h, μ_e) for $GdGa_2$ and $TbGa_2$ are summarized in Fig. 4. Both materials exhibit systematic suppression of carrier mobility with increasing temperature, attributable to enhanced electron–phonon scattering. While $GdGa_2$ shows an overall increase in carrier density with increasing temperature, $TbGa_2$ exhibits an increase in electron density (n_e) accompanied by a decrease in hole density (n_h). These results may not fully reflect the intrinsic carrier parameters in the antiferromagnetic state, as possible contamination from the anomalous Hall effect component proportional to the magnetization M cannot be excluded (see the discussion in the next section). Future studies employing angle-resolved photoemission spectroscopy and *ab initio* band-structure calculations are needed to elucidate the electronic structure of $REGa_2$.

3.3. Hall anomalies and magnetic phase diagram in $GdGa_2$

In metallic systems, the Hall resistivity ρ_{xy} can generally be decomposed as

$$\rho_{xy} = \rho_{xy}^{O} + \Delta\rho_{xy} = \rho_{xy}^{O} + \rho_{xy}^{A} + \rho_{xy}^{T}, \tag{4}$$

where ρ_{xy}^{O}, ρ_{xy}^{A}, and ρ_{xy}^{T} denote the ordinary, anomalous, and topological Hall resistivities, respectively.[24] As noted in the previous section, $\rho_{xy}(H)$ and $\rho_{xx}(H)$ in $GdGa_2$ exhibit kinks around $\mu_0 H \sim 4$ T at $T = 2$ K, precluding reliable two-band fitting in the adjacent field range (2.5–5.5 T). Given the consistency of ordinary Hall behavior with the two-band model in the paramagnetic state, segmented fits were therefore performed below 2.5 T and above 5.5 T. The model accurately describes the data in these regimes (Fig. 5(a), thick red curves). Extrapolating these parameters to the full field range 0–7 T reveals pronounced deviations between experimental and fitted ρ_{xy} in the intermediate-field region, particularly at $T = 2$ K (Fig. 5(a), thin red curve). We use $\Delta\rho'_{xy}$ to quantify these deviations (Fig. 5(b)). Applying the same analysis procedure to data collected from 2 K to 15 K, the intermediate-field anomaly in $|\Delta\rho'_{xy}|$ is found to be suppressed above $T = 6$ K (Fig. 5(c)). Between 2 K and 6 K, the peak values of $|\Delta\rho'_{xy}|$ decrease monotonically with increasing temperature.

Figures 5(d) and 5(e) present the temperature-dependent evolution of magnetization (M) and magnetoresistance (MR) from 2 K to 12 K under applied magnetic fields H. A weak magnetic hysteresis emerges in $M(H)$ between 2 K and 6 K, accompanied by kink-like features in MR within the intermediate-field region. The anomalous Hall resistivity ρ_{xy}^{A} typically scales with M, $\rho_{xx}M$, or $\rho_{xx}^{2}M$. Over the field range investigated here, $M(H)$ exhibits predominantly linear behavior with an approximately constant slope despite the presence of hysteresis (Fig. 5(d)). Consequently, ρ_{xy}^{A} may also contribute a field-linear background. As a result, the two-band fit may not capture the genuine ρ_{xy}^{O}, and $\Delta\rho'_{xy}$ may therefore not correspond exactly to $\Delta\rho_{xy}$ in Eq. (4). Nevertheless, the temperature and field dependence of the Hall anomalies remains unaffected. The intermediate-field Hall anomaly $\Delta\rho'_{xy}$ exhibits a characteristic nonmonotonic field dependence, increasing and then decreasing with magnetic field. Such behavior cannot be explained by the conventional anomalous Hall effect, which typically varies monotonically with field, and instead originates predominantly from the topological contribution ρ_{xy}^{T}, superimposed on an incompletely subtracted linear background.

We define the critical fields H_{c1} and H_{c2} as the onset and termination points of the magnetic hysteresis at low and high fields, respectively. The corresponding kink positions in

MR are identified in the same manner. These critical fields, combined with the temperature-dependent $|\Delta\rho'_{xy}|$ data shown as background colormaps, are used to construct the magnetic phase diagram presented in Fig. 5(f). Notably, the region between H_{c1} and H_{c2} coincides with enhanced $|\Delta\rho'_{xy}|$ values (red regions), reminiscent of the A-phases reported in Ref. [25] — specifically the entire A1-phase and part of the A2-phase. Reference [25] identified these A-phases via REXS measurements within approximately 3–7 T and at temperatures below 25 K, suggesting multi-$\boldsymbol{q}$ cycloidal spin textures that may form a Néel-type skyrmion lattice. The Hall anomalies observed here thus provide transport evidence for the possible existence of magnetic skyrmions in $GdGa_2$. Further verification using magnetic force microscopy or spin-polarized scanning tunneling microscopy is therefore highly desirable.[30] Compared to the maximum transverse topological Hall resistivity ρ_{xy}^{T} reported for centrosymmetric antiferromagnets Gd_2PdSi_3 (2.6 $\mu\Omega\cdot$cm)[20] and $GdRu_2Si_2$ (0.3 $\mu\Omega\cdot$cm),[16] $GdGa_2$ exhibits a relatively small Hall anomaly amplitude of 0.07 $\mu\Omega\cdot$cm. Although Ref. [25] reports an extremely short magnetic period of only 0.54 nm for $GdGa_2$, the estimated skyrmion sizes in Gd_2PdSi_3 and $GdRu_2Si_2$ are approximately 2.5 nm and 1.9 nm, respectively,[16–20] which fall within the large-skyrmion regime.[31] If $GdGa_2$ lies in the small-skyrmion regime, its Hall resistivity is expected to decrease with reducing skyrmion size, whereas in the large-skyrmion regime the Hall resistivity increases as the skyrmion size decreases.[32]

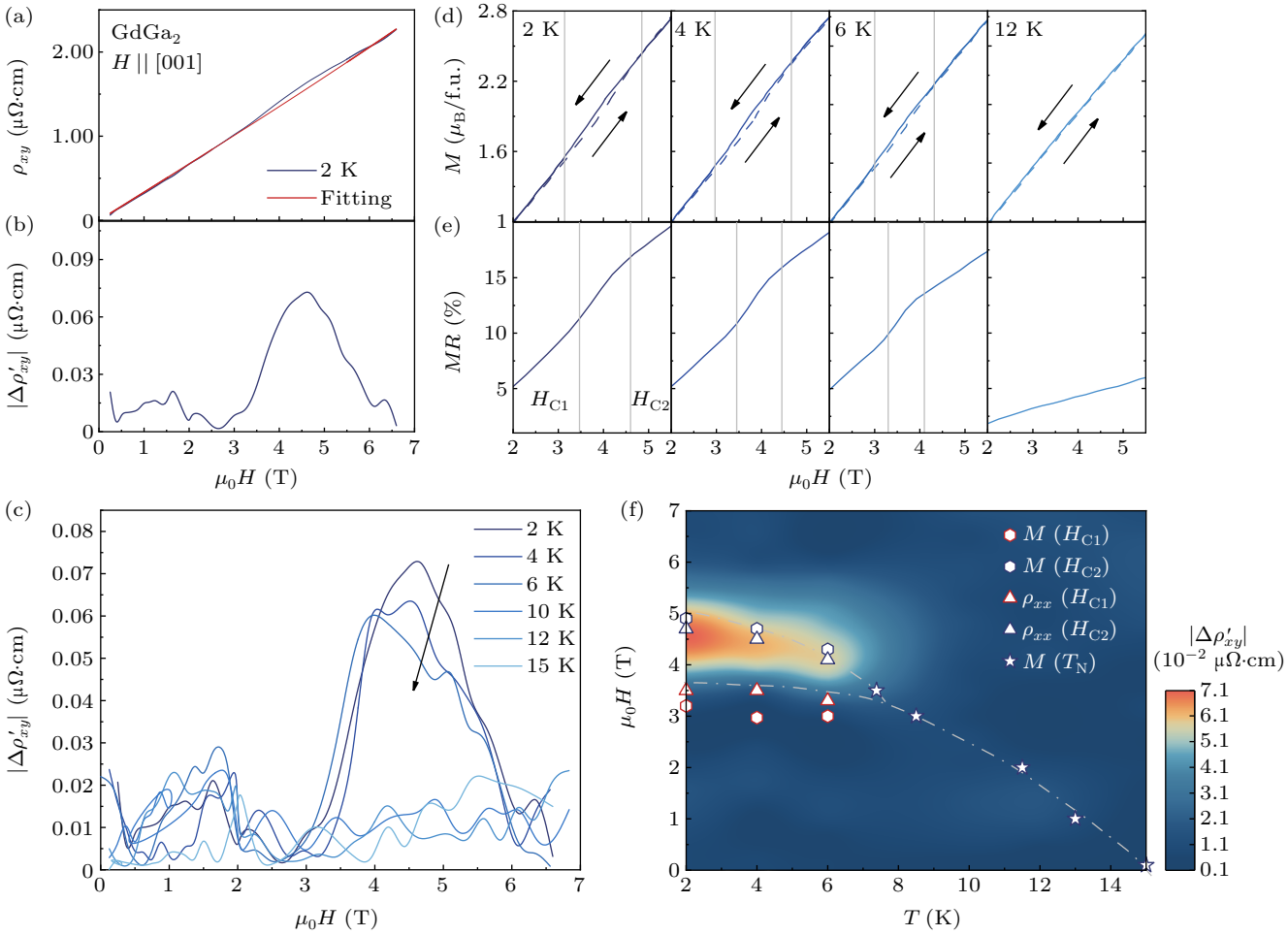


Fig. 5. (a) Hall resistivity $\rho_{xy}(H)$ of $GdGa_2$ at $T = 2$ K ($H \parallel c$). Thick red curve shows the two-band fit for $\mu_0 H < 2.5$ T and > 5.5 T using Eqs. (2) and (3). Thin red curve represents the extrapolation to the full field range (0–7 T). (b) Absolute residual $|\Delta\rho'_{xy}|$ at 2 K. (c) Temperature-dependent $|\Delta\rho_{xy}(H)'|$ for $GdGa_2$. Arrows indicate the direction of increasing temperature. (d) Magnetization $M(H)$ hysteresis at the indicated temperatures (solid: descending field; dashed: ascending field). Grey lines mark the critical fields H_{c1} and H_{c2}. (e) Magnetoresistance $MR(H)$ at selected temperatures. Grey lines indicate kink positions corresponding to H_{c1} and H_{c2}. (f) Magnetic phase diagram with $|\Delta\rho'_{xy}|$ shown as a colormap. The color scale is optimized to highlight regions with enhanced $|\Delta\rho'_{xy}|$. Phase boundaries, denoted by dashed grey lines, are estimated visually and serve as a guide to the eye. The enhancement of $|\Delta\rho'_{xy}|$ within the H_{c1}–H_{c2} range aligns with the A-phase region, consistent with the A1- and partially the A2-phases reported in Ref. [25].

In the low-temperature and low-field phase of $GdGa_2$, a further transition to phase I with crystallographic distortion and concomitant domain formation was reported in Ref. [25] based on magnetization and thermal expansion measurements. We do not observe evidence for this transition. This discrepancy may arise from growth-dependent magnetic properties: the Bridgman-grown crystals in Ref. [25] versus our Pb-flux-grown samples likely possess distinct defect densi-

ties and strain states, potentially affecting subtle phase transitions in magnetization. Importantly, this does not compromise the analysis of possible skyrmion-induced transport anomalies within the A-phases of $GdGa_2$.

It has been proposed that skyrmions in centrosymmetric materials, primarily Gd- and Eu-based rare-earth magnets, arise due to magnetic frustration, with spin anisotropy also possibly contributing.[23,33] Frustration in these magnets originates from the competition among short-range exchange interactions and/or long-range RKKY interactions in itinerant magnets, although which mechanism dominates remains controversial.[23,34–36] Recent studies on Gd_2PdSi_3 suggest that local Dzyaloshinskii-Moriya interactions, resulting from inversion symmetry breaking around Gd–Gd bonds due to inequivalent Pd–Si layer stacking, may also play a role despite the overall centrosymmetric crystal structure.[37] However, such a mechanism appears unlikely in ideally structured $GdGa_2$. In $GdGa_2$, conduction electrons interacting with possible skyrmions acquire a Berry phase, which manifests as an emergent magnetic field and gives rise to the Hall resistivity anomalies we observed.

4. Summary

In summary, we have systematically characterized the magnetic properties and electrical transport of $GdGa_2$ and $TbGa_2$ single crystals. Both compounds exhibit conventional two-band ordinary Hall behavior, while $GdGa_2$ displays additional field-induced Hall anomalies. The extracted topological contribution emerges in a region of the magnetic phase diagram that primarily coincides with the A1-phase previously determined by REXS, which is suggested to host a possible skyrmion lattice. Further confirmation of skyrmions in $GdGa_2$ will require local-probe techniques such as Lorentz transmission electron microscopy. These findings identify $GdGa_2$ as a new centrosymmetric rare-earth magnet candidate for hosting skyrmions and provide insights into unconventional skyrmion stabilization mechanisms.

Acknowledgment

This project was supported by the National Natural Science Foundation of China (Grant Nos. 12274125, 12574117, 12374105, and 12174103).

References

[1] Vojta M 2018 *Rep. Prog. Phys.* **81** 064501
[2] Broholm C, Cava R J, Kivelson S A, Nocera D G, Norman M R and Senthil T 2020 *Science* **367** eaay0668
[3] Tokura Y and Kanazawa N 2021 *Chem. Rev.* **121** 2857
[4] Fert A, Reyren N and Cros V 2017 *Nat. Rev. Mater.* **2** 17031
[5] Zhang Y S, Tang J, Wu Y D, Shi M, Xu X T, Wang S G, Tian M L and Du H F 2024 *Nat. Commun.* **15** 3391
[6] Tang J, Wu Y D, Jiang J L, Kong L Y, Liu W Y, Liu W, Wang S G, Tian M L and Du H F 2023 *Sci. Bull.* **68** 2919
[7] Tang J, Wu Y D, Wang W W, Kong L Y, Lv B Y, Wei W S, Zang J D, Tian M L and Du H F 2021 *Nat. Nanotechnol.* **16** 1086
[8] Wei W S, He Z D, Qu Z and Du H F 2021 *Rare Met.* **40** 3076
[9] Bak P and Jensen M H 1980 *J. Phys. C: Solid State Phys.* **13** L881
[10] Wilhelm H, Baenitz M, Schmidt M, Rößler U K, Leonov A A and Bogdanov A N 2011 *Phys. Rev. Lett.* **107** 127203
[11] Sutcliffe P 2017 *Phys. Rev. Lett.* **118** 247203
[12] Takagi R, Matsuyama N, Ukleev V, Yu L, White J S, Francoual S, Mardegan J R L, Hayami S, Saito H, Kaneko K, Ohishi K, Ōnuki Y, Arima T, Tokura Y, Nakajima T and Seki S 2022 *Nat. Commun.* **13** 1472
[13] Shang T, Xu Y, Gao S, Yang R, Shiroka T and Shi M 2024 *J. Phys.: Condens. Matter* **37** 013002
[14] Shang T, Xu Y, Gawryluk D J, Ma J Z, Shiroka T, Shi M and Pomjakushina E 2021 *Phys. Rev. B* **103** L020405
[15] Zhang H, Zhu X Y, Xu Y, Gawryluk D J, Xie W, Ju S L, Shi M, Shiroka T, Zhan Q F, Pomjakushina E and Shang T 2022 *J. Phys.: Condens. Matter* **34** 034005
[16] Khanh N D, Nakajima T, Yu X, Gao S, Shibata K, Hirschberger M, Yamasaki Y, Sagayama H, Nakao H, Peng L, Nakajima K, Takagi R, Arima T, Tokura Y and Seki S 2020 *Nat. Nanotechnol.* **15** 444
[17] Yasui Y, Butler C J, Khanh N D, Hayami S, Nomoto T, Hanaguri T, Motome Y, Arita R, Arima T, Tokura Y and Seki S 2020 *Nat. Commun.* **11** 5925
[18] Hirschberger M, Nakajima T, Gao S, Peng L, Kikkawa A, Kurumaji T, Kriener M, Yamasaki Y, Sagayama H, Nakao H, Ohishi K, Kakurai K, Taguchi Y, Yu X, Arima T and Tokura Y 2019 *Nat. Commun.* **10** 5831
[19] Ogunbunmi M O, Nair H S and Strydom A M 2022 *Crit. Rev. Solid State Mater. Sci.* **48** 480
[20] Kurumaji T, Nakajima T, Hirschberger M, Kikkawa A, Yamasaki Y, Sagayama H, Nakao H, Taguchi Y, Arima T and Tokura Y 2019 *Science* **365** 914
[21] Paddison J A M, Rai B K, May A F, Calder S, Stone M B, Frontzek M D and Christianson A D 2022 *Phys. Rev. Lett.* **129** 137202
[22] Hirschberger M, Hayami S and Tokura Y 2021 *New J. Phys.* **23** 023039
[23] Kawamura H 2025 *J. Phys.: Condens. Matter* **37** 183004
[24] Nagaosa N, Sinova J, Onoda S, MacDonald A H and Ong N P 2010 *Rev. Mod. Phys.* **82** 1539
[25] Baral P R, Khanh N D, Gen M, Sagayama H, Nakao H, Arima T H, Ōnuki Y, Tokura Y and Hirschberger M 2025 *J. Phys. Soc. Jpn.* **94** 024705
[26] Kurumaji T, Fang S, Ye L, Kitou S and Checkelsky J G 2024 *Proc. Natl. Acad. Sci.* **121** e2318411121
[27] Khatua J, Sana B, Zorko A, Gomilšek M, Sethupathi K, Rao M S R, Baenitz M, Schmidt B and Khuntia P 2023 *Phys. Rep.* **1041** 1
[28] Ohara S, Sakamoto I, Aoki Y, Sato H, Oguro I, Sasaki T, Kido G and Maruno S 1996 *Phys. B* **223** 379
[29] Hamasaki T, Yokoo T, Arai M, Ohara S and Sakamoto I 2004 *J. Magn. Magn. Mater.* **272** E465
[30] Oka H, Brovko O O, Corbetta M, Stepanyuk V S, Sander D and Kirschner J 2014 *Rev. Mod. Phys.* **86** 1127
[31] Hamamoto K, Ezawa M and Nagaosa N 2015 *Phys. Rev. B* **92** 115417
[32] Matsui A, Nomoto T and Arita R 2021 *Phys. Rev. B* **104** 174432
[33] Gomilšek M, Hicken T J, Wilson M N, Franke K J A, Huddart B M, Štefančič A, Holt S J R, Balakrishnan G, Mayoh D A, Birch M T, Moody S H, Luetkens H, Guguchia Z, Telling M T F, Baker P J, Clark S J and Lancaster T 2025 *Phys. Rev. Lett.* **134** 046702
[34] Leonov A O and Mostovoy M 2015 *Nat. Commun.* **6** 8275
[35] Dong Y, Arai Y, Kuroda K, Ochi M, Tanaka N, Wan Y, Watson M D, Kim T K, Cacho C, Hashimoto M, Lu D, Aoki Y, Matsuda T D and Kondo T 2024 *Phys. Rev. Lett.* **133** 016401
[36] Bouaziz J, Mendive-Tapia E, Blügel S and Staunton J B 2022 *Phys. Rev. Lett.* **128** 157206
[37] Moody S H, Bereciartua P J, Francoual S, Littlehales M T, Wilson M N, Gomilšek M, Birch M T, Mayoh D A, Balakrishnan G and Hatton P D 2025 *Phys. Rev. Lett.* **135** 076706